Yongming Wang, Qingde Chen* and Xinghai Shen*

Radiolytic syntheses of hollow UO_2 nanospheres in Triton X-100-based lyotropic liquid crystals

DOI 10.1515/ract-2016-2626
Received April 29, 2016; accepted November 7, 2016; published online December 19, 2016

Abstract: Hollow nanospheres (ϕ: 60–80 nm, wall thickness: 10–20 nm), consisted of UO_2 nanoparticles (ϕ: 3–5 nm), were successfully prepared in a Triton X-100-water (50 : 50, w/w) hexagonal lyotropic liquid crystal (LLC) by γ-irradiation, where water soluble ammonium uranyl tricarbonate was added as precursor. The product was stable at least up to 300 °C. Furthermore, whether the nanospheres were hollow or not, and the wall thickness of the hollow nanospheres could be easily controlled *via* adjusting dose rate. While in the Triton X-100 based micellar systems, only solid nanospheres were obtained. At last, a possible combination mechanism containing adsorption, aggregation and fracturing processes was proposed.

Keywords: Hollow UO_2 nanospheres, lyotropic liquid crystal, Triton X-100, γ-irradiation, ammonium uranyl tricarbonate.

1 Introduction

Uranium oxides, including UO_2, UO_3, U_3O_8 and so on, are a class of important nuclear materials. Besides, uranium oxides are able to catalyze some important reactions, such as the destruction of volatile organic compounds by using U_3O_8 [1], the dehydration of ethanol by using UO_2 [2], and the formation of furan from acetaldehyde by using UO_3 [3]. In the last decade, some nano-sized uranium oxides were found to have a much better catalytic performance [4–6]. Thus, uranium oxide nanomaterials have attracted much attention. Up to now, quasi-spherical UO_2 nanoparticles [5, 7–9], flower-like U_3O_8 nanostructures [6], U_3O_8 nanorods [5, 10], U_3O_8 nanotubes [11], hierarchical uranium oxides nano/microspheres [6, 12] have been obtained by thermochemical and electrochemical methods. In the field of catalysis, uniform hollow spheres with nanometer-to-micrometer dimensions have been of intense interest for their tailored structural, mechanical, surface and penetration properties [13–15]. However, to the best of our knowledge, there have been no any reports about the formation of hollow uranium oxides spheres. Therefore, it is essential to synthesize hollow uranium oxides nano/microspheres, favoring the exploration in the field of catalysis.

Lyotropic liquid crystal (LLC), composed of certain surfactants and solvents, has been widely used to deliver drug [16], fabricate nanoparticles [17, 18] and so on for their ordered internal structures. In the field of nanoscience and technology, LLCs have been extensively applied to synthesize mesoporous structures with highly ordered networks and narrow pore-size distributions [18–20], as well as nanofilms [17, 21], nanorods [17, 22], and nanowires [17, 18] by chemical or electrochemical reduction. Recently, it was found that nanotubes could be formed *via* the rolling-up of the nanosheets synthesized by LLC with lamellar structure [23, 24]. Zhang et al. [25] have ever got hollow silica nanospheres in AOT/H_2O lamellar liquid crystal with the assistance of compressed CO_2. Nevertheless, in the presence of compressed CO_2, the lamellar liquid crystal was switched into micellar solution, as the actual template [25]. Thereby, there is a great challenge in the fabrication of hollow nano/microspheres and the exploration of its new mechanism in LLC systems.

Ionizing radiation (such as γ-irradiation, electron irradiation and so on) has been widely used in the syntheses of nanoparticles [26, 27]. Herein, we attempt to control the synthesis of hollow uranium oxides nano/microspheres by using basic $UO_2(CO_3)_3^{4-}$ as precursor in Triton X-100-based hexagonal LLCs by γ-irradiation. On the one hand, Jiang and collaborators [28] prepared ZnS nanowires in an inverted hexagonal liquid crystal formed by polyoxyethylene (10) oleyl ether, *n*-hexane, *n*-hexanol/*i*-propanol (2 : 1),

***Corresponding authors: Qingde Chen and Xinghai Shen,** Beijing National Laboratory for Molecular Sciences, Fundamental Science on Radiochemistry and Radiation Chemistry Laboratory, College of Chemistry and Molecular Engineering, Peking University, Beijing 100871, P. R. China, Phone: 86-10-62755200, Fax: 86-10-62759191, E-mail: qdchen@pku.edu.cn (Q. Chen); and Phone: 86-10-62765915, Fax: 86-10-62759191, E-mail: xshen@pku.edu.cn (X. Shen)
Yongming Wang: Beijing National Laboratory for Molecular Sciences, Fundamental Science on Radiochemistry and Radiation Chemistry Laboratory, College of Chemistry and Molecular Engineering, Peking University, Beijing 100871, P. R. China

and water. As far as we know, this is the only one report about the combination of ionizing radiation and LLCs. In this direction, more work is very necessary. On the other hand, the UO_2 sol has been obtained under acidic conditions by ionizing radiation [29–31]. Recently, the work by Rath and co-workers indicated that the UO_2 sol synthesized by radiolytic method were easily oxidized in air atmosphere [31]. Thus, there are still many problems awaiting resolution.

In the last decade, we tried our best to extend the application of ionizing radiation in nanoscience and nanotechnology. By far, mesoporous $BaSO_4$ microspheres [32], octahedron Cu_2O nanocrystals [33], solid and hollow Cu_2O nanocubes [34], and prismatical $PbSO_4$ microcrystals [35] have been successfully synthesized. In the present work, we attempt to reveal a possible new mechanism *via* the radiolytic syntheses of hollow uranium oxides nano/microspheres in Triton X-100-based hexagonal LLCs.

2 Experimental

2.1 Chemicals

$UO_2(NO_3)_2{\cdot}6H_2O$ (G.R., Chemapol, Prague Czechoslovakia), Triton X-100 [$(CH_3)_3CCH_2C(CH_3)_2C_6H_4(OCH_2CH_2)_{10}OH$, CP, Beijing Chemical Reagents Inc.] were used as received. NH_4HCO_3, Na_2CO_3 and ethanol were of A.R. grade and were used without further purification. Ultrapure water was used throughout the experiments.

2.2 Synthesis of ammonium uranyl tricarbonate

According to Ref. [36], ammonium uranyl tricarbonate (AUC) crystal was prepared. $UO_2(NO_3)_2{\cdot}6H_2O$ was heated in a muffle furnace at 350 °C, then an orange-yellow powder was obtained, i. e. uranium trioxide. The saturated NH_4HCO_3 solution was added slowly into the flask containing the uranium trioxide powder with constant stirring and reflux at 60 °C until a yellow and clear solution was gotten. When the solution cooled to room temperature, a yellow AUC was precipitated from the solution. The result of element analysis was identical with the theoretical value. Elemental analysis: calcd (%) for $(NH_4)_4[UO_2(CO_3)_3]$ (522.21): C 6.90, H 3.09, N 10.73; found: C 6.87, H 3.09, N 10.70.

2.3 Synthesis of nanospheres

A certain amount of AUC was dissolved in water to make up a 5 mmol·L^{-1} solution. To stabilize the solution, 15 mmol·L^{-1} Na_2CO_3 was added simultaneously. Then, the solution and Triton X-100 in certain weight ratio were mixed adequately by vortex. After bubbling with high pure N_2 for 20 min, the mixtures were irradiated in the Peking University's Gamma Irradiation Facility using ^{60}Co γ-ray source for a definite time at a special location whose dose rate was determined by a ferrous sulfate dosimeter. By monitoring, the temperature of the irradiation room was not above 18 °C in the irradiation course. After irradiation, black mixtures were obtained.

2.4 Characterization

The mixtures of Triton X-100 and AUC aqueous solution before and after γ-irradiation were detected on a Leica DMLP polar microscope (POM) and an AntonPar SAXSess small angle X-ray scattering system (SAXS) at ambient temperature (*ca*. 18 °C). The micellar mixture of 25 wt% Triton X-100 and AUC aqueous solution was characterized on a Malvern Nano ZS90 instrument at 25 °C and at a scattering angle of 90°. A He-Ne laser with a power of 4 mW was used as a light source. Before the measurement, the samples were centrifugated at 10000 rpm for 30 min.

After irradiation, the obtained black mixtures were washed by ethanol and water in turn, until there was not the absorption of phenyl group in the UV-visible spectra of the washing liquid. Then, the black powders were dried in a vacuum oven overnight at room temperature. The well washed powders were dispersed in water, and were dropped onto a carbon-coated copper grid. After the solvent was evaporated at room temperature, the transmission electron microscopy (TEM), the selected area electron diffraction (SAED) and the high-resolution TEM (HRTEM) were obtained on a FEI Tacnai G2 T20 microscope operated at 200 kV. Scanning electron spectroscopy (SEM) image was obtained by a FEI nanoSEM 430 scanning electron microscope operated at 15 kV. The range of particle size was determined by measuring the dimensions of more than 100 particles. Powder X-ray diffraction (XRD) pattern was recorded on a Rigaku Dmax-2000 diffractometer with Cu Kα radiation ($\lambda = 0.15418$ nm) and X-ray photoelectron spectrum (XPS) was collected on a Kratos Axis Ultra spectrometer with monochromatized Al Kα radiation.

3 Results and discussion

3.1 Effect of AUC on the phase behavior of Triton X-100-based LLC

The phase behavior of Triton X-100 and water binary system has been well characterized. Among the mixtures, there exists a columnar hexagonal phase at Triton X-100 content of 40–55 wt% at 18 °C, and a lamellar phase at Triton X-100 content of 70 wt% below 8 °C [37].

The mixture doping with $UO_2(CO_3)_3^{4-}$ at a Triton X-100 content of 50 wt% was still liquid crystal. The optical texture observed by POM was fanlike (Figure 1a), similar to that reported in the literature [38, 39] and that of the mixture before doping (Figure SI-1, Supporting Information). Furthermore, in the related SAXS spectrum (curve a, Figure 2), there appeared three peaks with scattering factor (q) ratio of $1:\sqrt{3}:\sqrt{4}$, corresponding to the (100), (110) and (200) planes of a hexagonal LLC [28].

At a Triton X-100 content of 70 wt%, the fluxible mixture became more viscous after doping with $UO_2(CO_3)_3^{4-}$, and a typical Maltese crosses optical texture appeared in the POM image (Figure 1c), indicating the appearance of lamellar LLC [40, 41]. In other words, the phase regions of the Triton X-100-based lamellar LLCs were extended to some extent *via* doping with water soluble AUC. Celik and Dag [42] have ever found that the polyoxyethylene chain of $C_{12}H_{25}(OCH_2CH_2)_{10}OH$ can form hydrogen bonds with transition metal aqua complexes. Herein, the enlargement of the lamellar phase regions may be ascribed to the interaction between UO_2^{2+} and the polyoxyethylene chain in Triton X-100.

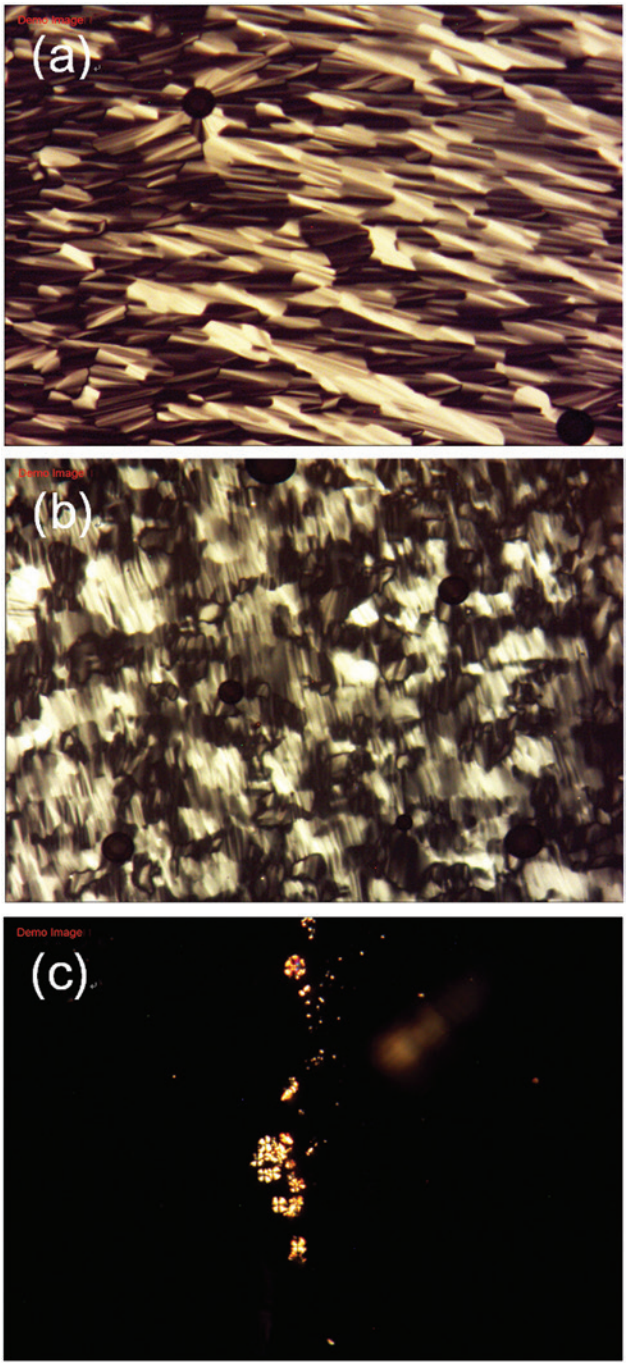

Figure 1: POM images (×200) of the LLC samples doping with $UO_2(CO_3)_3^{4-}$ before (a and c) and after (b) irradiation at 18 °C. Triton X-100 content: (a and b) 50 wt%, (c) 70%. The dose rate is 40 Gy·min^{-1}, and the absorbed dose is 12 kGy.

3.2 Characterization of hollow UO_2 nanospheres

Figure 3a, b shows the TEM and SEM images of the sample prepared in the liquid crystal system at Triton X-100 content of 50 wt% by γ-irradiation at a dose rate of 40 Gy·min^{-1} for 300 min. It can be seen that the product is composed of nanospheres with a diameter of 60–80 nm. Besides, as for most nanospheres, it seems that the brightness of the edge is different from that of the center (Figure 3a). The TEM image in higher magnification (Figure 3c) further shows a distinct contrast between the dark edge and the pale center, evidencing their hollow nature. The wall thickness is estimated to be 10–20 nm.

The related SAED pattern (inset, Figure 3c) exhibits four diffraction rings with plane distance of 0.314, 0.277, 0.195 and 0.166 nm, consistent with the cubic phase UO_2 (111), (200), (220) and (311) plane distances of 0.3153, 0.2733, 0.1933 and 0.1647 nm (JCPDS file No. 41-1422). This confirms the formation of polycrystalline UO_2 nanospheres. The corresponding XRD analysis (curve a, Figure 4), accordant with the cubic phase UO_2, further validates the generation of UO_2. Moreover, the broadened diffraction peaks (curve a,

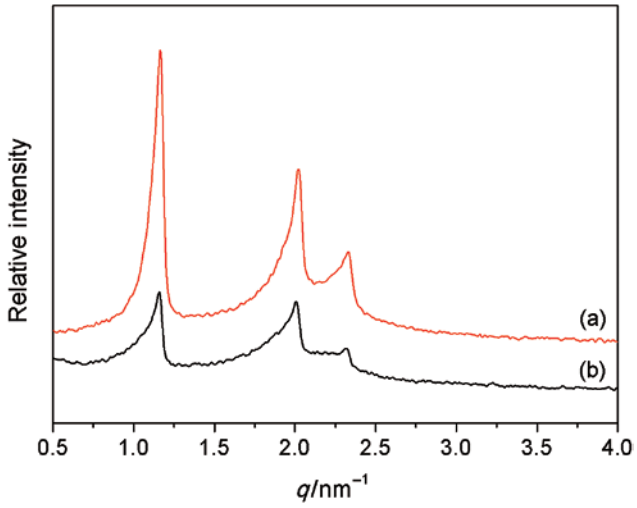

Figure 2: SAXS spectra of the LLC samples doping with $UO_2(CO_3)_3^{4-}$ before (a) and after (b) irradiation at 18 °C. Triton X-100 content: 50 wt%. The dose rate is 40 Gy·min^{-1}, and the absorbed dose is 12 kGy.

Figure 4) suggests that the hollow UO_2 nanospheres consist of nanoparticles, which is verified by the enlarged TEM image (Figure 3c). Furthermore, the related HRTEM image shown in Figure 3d indicates the diameter of the individual nanoparticles was about 3–5 nm. It is noteworthy that the *d* spacing of most lattice fringes is 0.34 nm, which does not coincide with any interplanar distances of UO_2 crystal, but corresponds to (130), (111) or (200) reflection of α-U_3O_8 crystal (JCPDS file No. 31-1424), (110) reflection of α′-U_3O_8 crystal (JCPDS file No. 31-1425), (105) reflection of tetragonal γ-UO_3 structure (JCPDS file No. 31-1421), or (151) reflection of orthorhombic γ-UO_3 structure (JCPDS file No. 31-1422). This hints the existence of U_3O_8 or UO_3 on the surface of nanospheres. Nevertheless, the diffraction peaks corresponding to U_3O_8 or UO_3 cannot be obviously observed in the XRD pattern (curve a, Figure 4), indicating their low content.

To get more information about the surface composition of the product, XPS analysis was carried out. Figure 5a presents the relevant XPS spectrum in U 4f region. Because of spin-orbit splitting, the peak of U 4f is divided into two peaks of U $4f_{5/2}$ and U $4f_{7/2}$ at the binding energies of 392.4 and 381.5 eV, respectively, close to the values of U(IV) or U(VI) reported in the literature [43]. Through peak-fitting analysis, it was found that the two U 4f peaks could be well fitted by two groups of peaks (Figure 5a). One group consists of U(VI) $4f_{5/2}$ peak at 392.5 eV and U(VI) $4f_{7/2}$ peak at 381.6 eV, while the

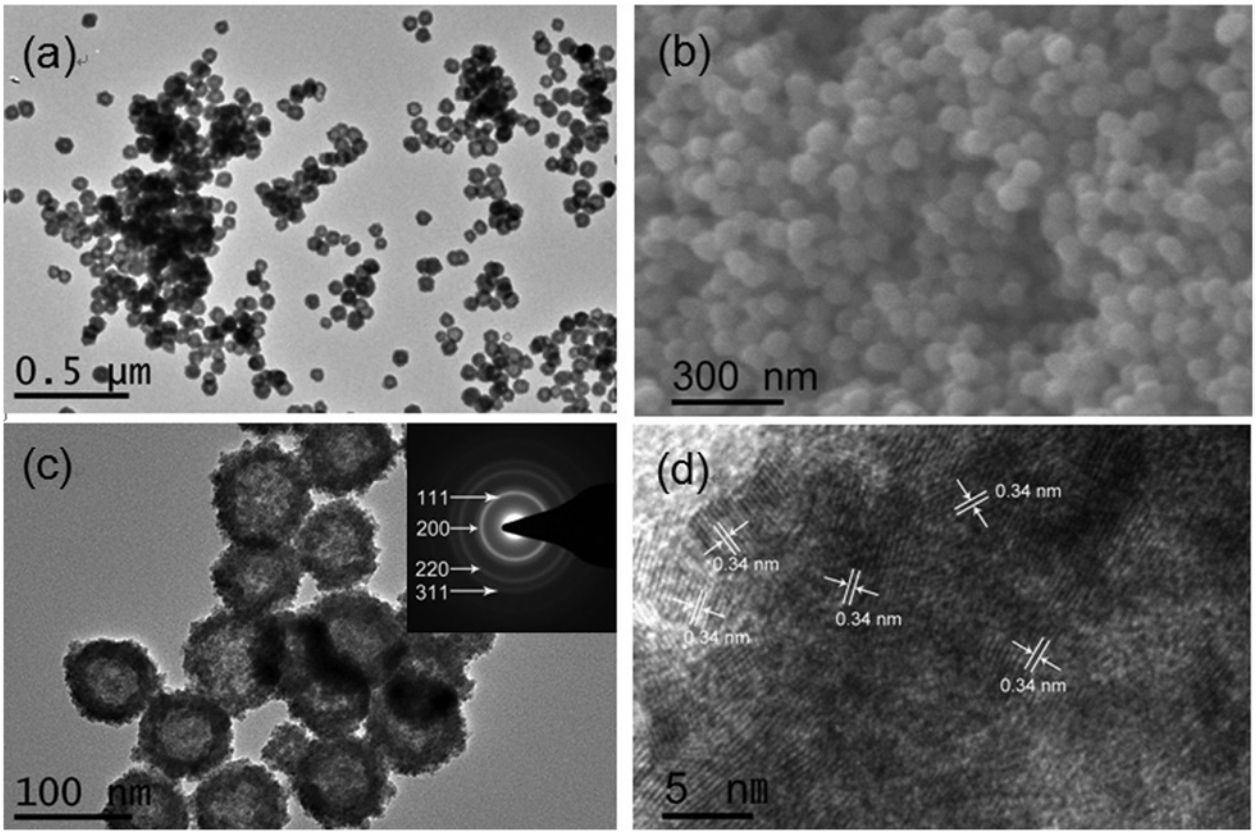

Figure 3: TEM (a and c), SEM (b) and HRTEM (d) images of the product synthesized in the LLC with a Triton X-100 content of 50 wt% at a dose rate of 40 Gy·min^{-1} for 300 min. The inset in (c) shows the SAED pattern of the corresponding product.

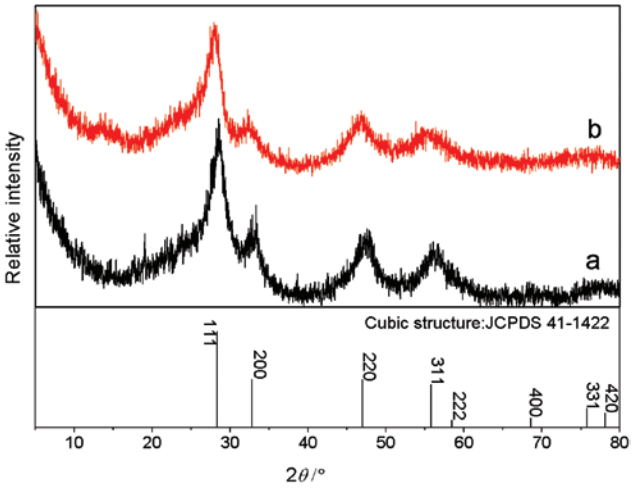

Figure 4: Powder XRD spectra of the product synthesized in the LLC with a Triton X-100 content of 50 wt% before (a) and after (b) calcination. In the irradiation course, the dose rate is 40 Gy·min^{-1}, and the absorbed dose is 12 kGy.

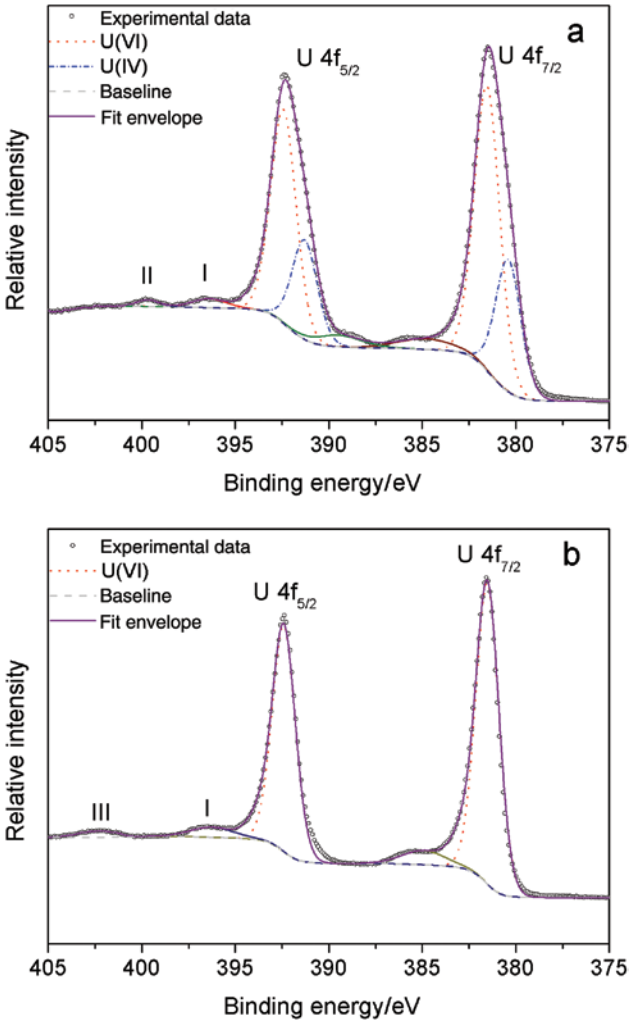

Figure 5: XPS patterns in the U 4f region of the products synthesized in the LLC with a Triton X-100 content of 50 wt% before (a) and after (b) calcination. In the irradiation course, the dose rate is 40 Gy·min^{-1}, and the absorbed dose is 12 kGy.

other group consists of U(IV) $4f_{5/2}$ peak at 391.3 eV and U(IV) $4f_{7/2}$ peak at 380.5 eV. In general, U $4f_{5/2}$ peak comes with some characteristic satellite peaks at a higher binding energy, and the binding energy difference (ΔE_{sp}) between the satellite peak and the main peak is constant with respect to some particular valence of uranium [43–45]. For example, the ΔE_{sp} value of U(VI) is *ca.* 3.8 and/or 9.4 eV, while that of U(IV) is *ca.* 8.2 eV. In the XPS spectrum (Figure 5a), there are two U $4f_{5/2}$ satellite peaks at the binding energies of 396.4 and 399.7 eV, respectively. The ΔE_{sp} value between peak I and U(VI) $4f_{5/2}$ peak is 3.9 eV, and that between peak II and U(IV) $4f_{5/2}$ peak is 8.4 eV, close to the literature values. The above results indicate the coexistence of U(VI) and U(IV) on the surface of nanospheres. Besides, the result of peak fitting discloses the presence of U(VI) and U(IV) in a molar ratio of 2.15 : 1.00, implying the presence of U_3O_8, or the coexistence of UO_3 and UO_2 in a molar ratio of 2.15 : 1. Because the lattice fringes of UO_2 was difficult to be observed in the HRTEM images, it was reasonable to conclude that the surface of the product was mainly comprised of U_3O_8 due to the surface oxidation of product exposed to air environment.

Therefore, we believe that the obtained black powder consisted of hollow UO_2 nanospheres, whose surface was U_3O_8 mainly.

3.3 Thermal stability of hollow UO_2 nanospheres

To examine the thermal stability of the obtained hollow UO_2 nanospheres, the well washed and dried products were calcinated in a muffle furnace at 300 °C in air atmosphere for 3 h. The TEM image (Figure 6a) shows that most of the hollow structures can be reserved after calcination. The XRD pattern (curve b, Figure 4) is consistent with the standard pattern of cubic phase UO_2, and there appear (111), (200), (220) and (311) diffraction rings corresponding to cubic phase UO_2 in the SAED pattern (inset, Figure 6a), which indicates that the product is stable at least up to 300 °C. According to the HRTEM image (Figure 6b) similar to that in Figure 3d, it seems that no change occurs on the surface. However, according to the related XPS analysis in U 4f region (Figure 5b), the two main peaks at 392.5 and 381.6 eV can be assigned to U(VI) $4f_{5/2}$ and $4f_{7/2}$ photoelectrons, respectively. It is worth noting that the peak II disappears. There appear peak I at 396.2 eV and peak III at 402.1 eV, which can be attributed to the satellite peaks of

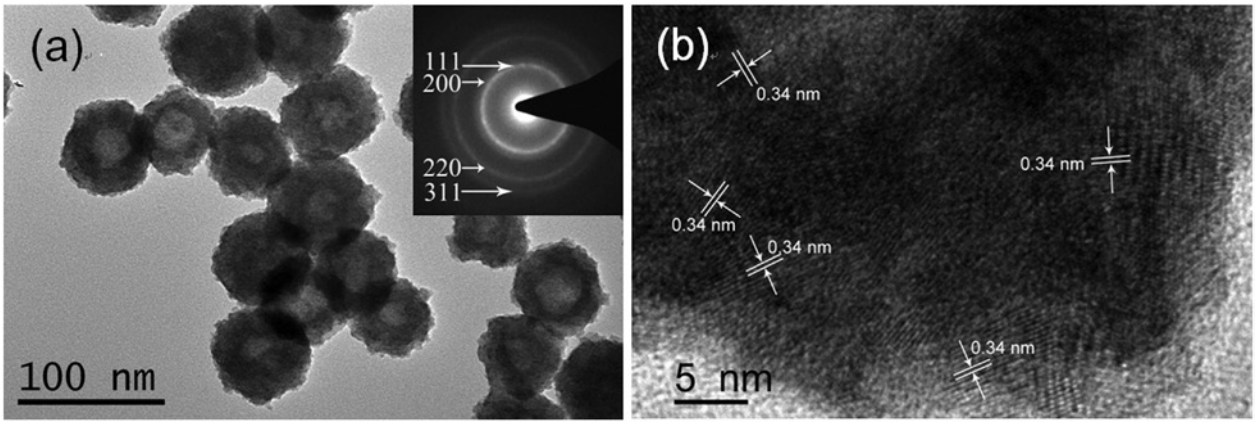

Figure 6: TEM (a) and HRTEM (b) image of the product after calcination. The sample before calcination was synthesized in the LLC with a Triton X-100 content of 50 wt% by γ-irradiation at a dose rate of 40 Gy·min^{-1} for 300 min. The inset in (a) shows the SAED pattern of the corresponding product.

U(VI) $4f_{5/2}$ peak for the corresponding ΔE_{sp} values of 3.7 and 9.6 eV, respectively. Thus, the surface composition of the calcinated product was UO_3 mainly. It might be the formation of UO_3 or U_3O_8 layer on the surface of the hollow nanospheres that prevent the inner UO_2 from oxidation.

3.4 Effect of dose rate

In the radiolytic syntheses, it is a powerful method to adjust the dose rate in controlling the size and morphology of nanoparticles. In the present work, the absorbed dose was fixed at 12 kGy. At a dose rate of 200 Gy·min^{-1} for 60 min, most of the obtained nanospheres is solid (Figure 7a). With the decrease of dose rate, the hollow nanospheres become the main product, and the wall becomes thinner gradually (Figures 3c, 7b and c). However, when the dose rate is decreased to 12 Gy·min^{-1}, solid nanospheres appear again, and the cavity of hollow nanospheres becomes smaller (Figure 7d). This indicates that the dose rate plays an important role in the formation of hollow nanospheres, and a dose rate between 40 and 70 Gy·min^{-1} is suitable to the formation of hollow nanospheres with a thin wall.

3.5 Effect of phase state

To answer the question of whether the Triton X-100 based LLCs play the role of template in the formation of hollow UO_2 nanospheres or not, the mixtures with different Triton X-100 contents, corresponding to various phase states, were irradiated at a dose rate of 70 Gy·min^{-1} for 171.4 min. In the literature, micelles were the widely used soft templates for the preparation of hollow nano/microspheres [13, 46, 47]. At the Triton X-100 content of 25 wt%, the mixture was a flowable micellar solution, where the average hydrodynamic radius of micelles was about 2 nm (Figure SI-2, Supporting Information). As shown, only solid nanospheres are obtained in the system (Figure 8a). Besides, in the other micellar region doping with lamellar LLC, the choice of the system with a Triton X-100 content of 70 wt% does not lead to the appearance of hollow structures, but only solid nanospheres are generated (Figure 8b). In other words, the Triton X-100 based hexagonal LLCs play a key role in the generation of hollow UO_2 nanospheres.

In the literature, the AOT/H_2O lamellar liquid crystal was switched into micellar solution with the assistance of compressed CO_2, which acted as template to prepare hollow silica nanospheres [25]. In the present work, the results of POM (Figure 1b) and SAXS (curve b, Figure 2) analyses indicate that the LLC with the Triton X-100 content of 50 wt% after irradiation still possesses of hexagonal structure. However, the optical texture becomes smaller (Figure 1b). Because the texture comes from the combination of the interference effect of defects and the discontinuous variation of the molecular orientation [48], this result implies the appearance of more defects and/or discontinuous structures.

3.6 Formation mechanism of hollow UO_2 nanospheres

As known, when a LLC is irradiated by γ-rays, many reactive species, such as e_{aq}^-, ·H and ·OH, are generated *via* the radiolysis of water (Eq. 1) [49].

$$H_2O \xrightarrow{\text{irradiated}} e_{aq}^-, H, \cdot OH, H_3O^+, \bullet\bullet\bullet \quad (1)$$

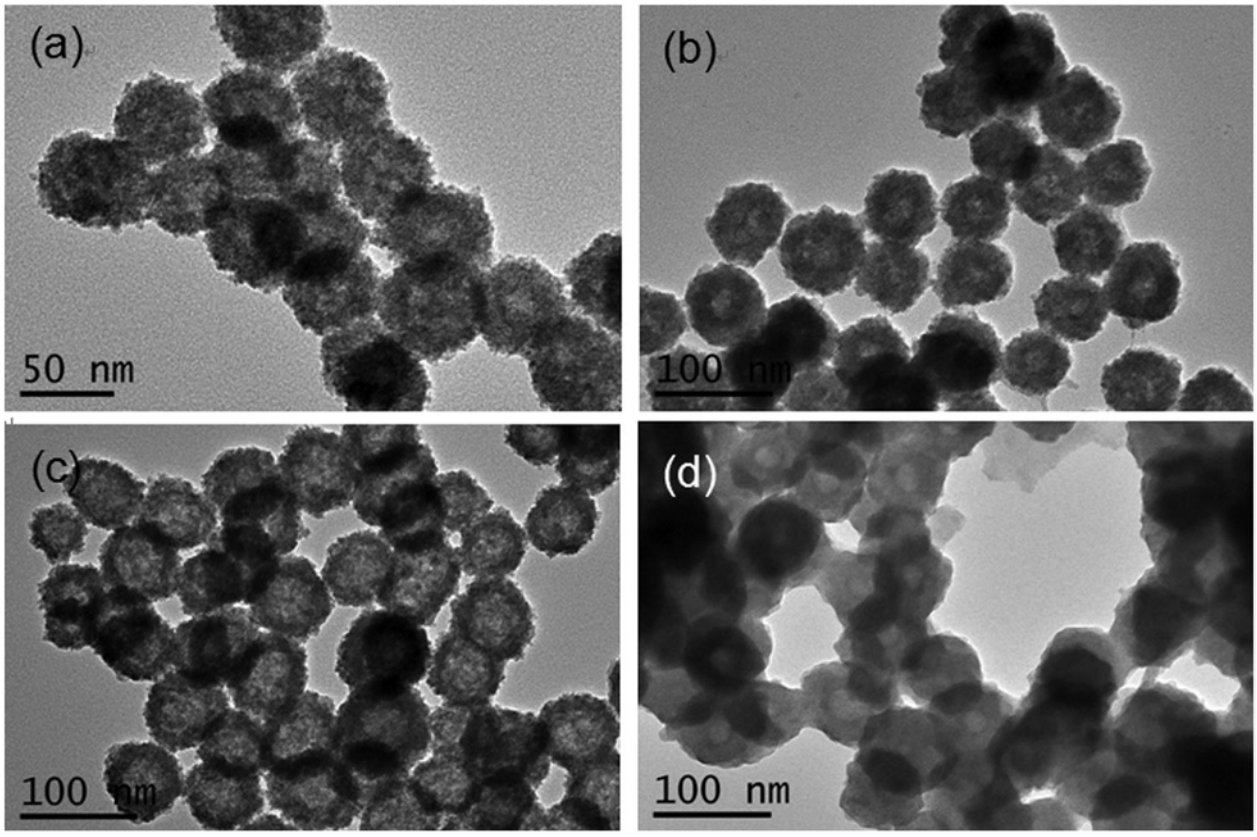

Figure 7: TEM images of the products prepared in LLC with a Triton X-100 content of 50 wt% at different dose rate: (a) 200 Gy·min^{-1}, (b) 100 Gy·min^{-1}, (c) 70 Gy·min^{-1}, (d) 12 Gy·min^{-1}. The absorbed dose is fixed at 12 kGy.

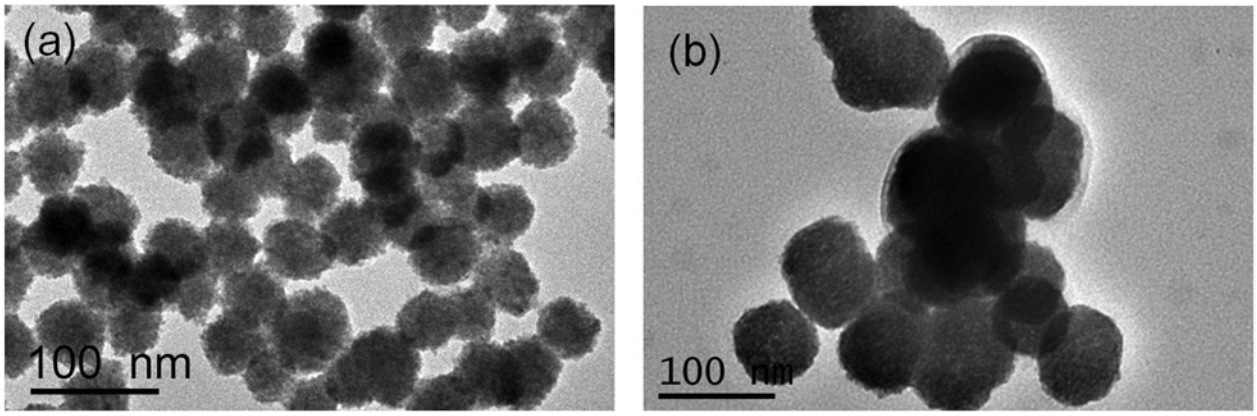

Figure 8: TEM images of the products prepared in LLC with different Triton X-100 content: (a) 25 wt%, (b) 70 wt%. In the irradiation course, the dose rate is 70 Gy·min^{-1}, and the absorbed dose is 12 kGy.

Meanwhile, the reducing species, especially e_{aq}^-, reduce the U(VI) in $UO_2(CO_3)_3^{4-}$ ions to U(IV) ions, which are precipitated in the form of $U(OH)_4$ by hydroxyl ions under the basic aqueous environment. Then, UO_2 is generated *via* the dehydration of $U(OH)_4$. While $UO_2(NO_3)_2$ was used as precursor, no product was obtained for the low pH value because the generated UO_2 and/or $U(OH)_4$ nanoparticles could be dissolved by H_3O^+. Furthermore, the oxidative ·OH could be eliminated by Triton X-100 with a rate constant of 6.4×10^9 L·mol^{-1}·s^{-1} in 10% Triton X-100 micellar solution [49]. Thus, the system could be kept in a reducing circumstance, favoring the reduction of U(VI) and the formation of nanoparticles.

During the fabrication of UO_2 nanospheres from the generated UO_2 and/or $U(OH)_4$ nanoparticles, there may

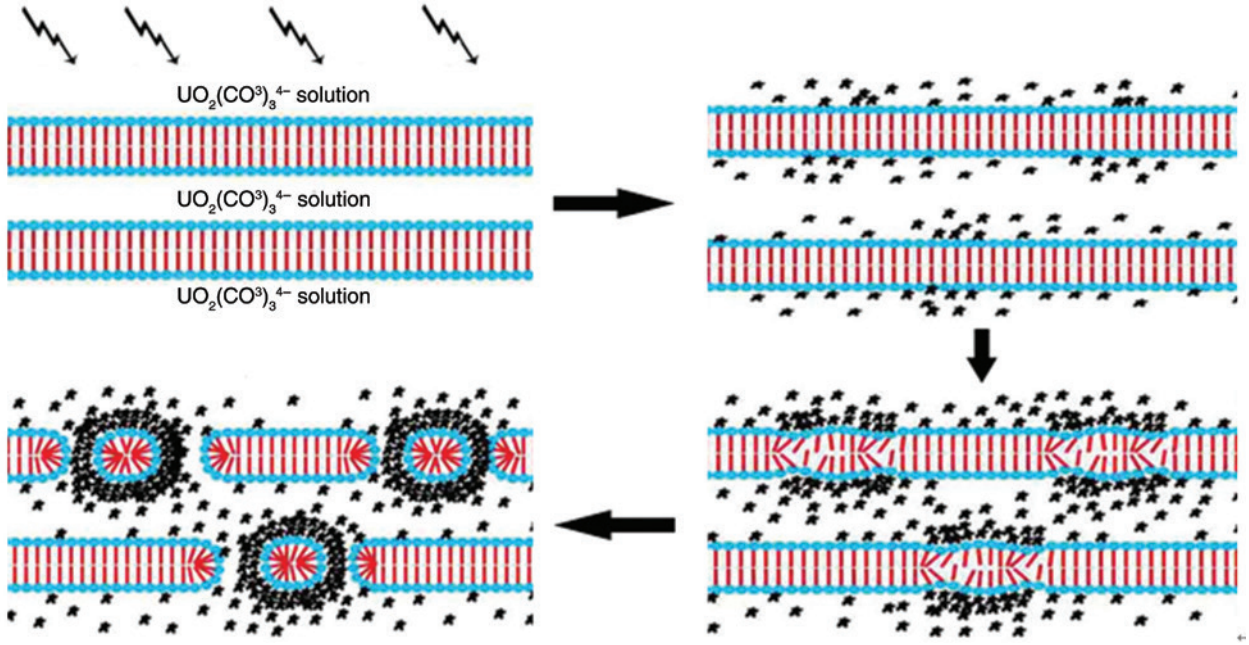

Scheme 1: Formation mechanism of hollow UO_2 nanospheres.

exist two competitive pathways. One follows a simple aggregation mechanism, the other follows a combination mechanism containing adsorption, aggregation and fracturing processes (Scheme 1).

At a higher dose rate (e. g. 200 Gy·min^{-1}), the generation of nanoparticles is too quick to be adsorbed by the polyoxyethylene chains of Triton X-100 distributed on the surface of the palisade layer. Thus, the simple aggregation mechanism plays a key role, leading to the generation of solid nanospheres.

While the dose rate decreases, the formation of nanoparticles becomes slower, which makes it possible for the nanoparticles to interact with the polyoxyethylene chains of Triton X-100 and be adsorbed on the surface of the palisade layer. Simultaneously, the aggregation of nanoparticles around the deposited ones takes place, which causes the uneven distribution of nanoparticles on the palisade layer. Because the Triton X-100-based hexagonal LLC only exists below 28 °C [37], the palisade layer may be not strong enough. Then, the fracture of the palisade layer happens, and the surfactants are encapsulated, which could be removed in the process of post-treatment. This results in the formation of hollow nanospheres and discontinuous LLC structures. With respect to the wall thickness, it may depend on the balance between the two processes, i. e. adsorption and aggregation.

When the dose rate decreases to some extent (e. g. 12 Gy·min^{-1}), the generation rate of nanoparticles decreases dramatically. At this time, another process, i. e. the escape of surfactants, begins to compete with the above processes, causing the appearance of solid nanospheres and/or nanospheres with a smaller cavity. This process is similar to the case reported in the literature, which produced hollow Cu_2O nanostructures *via* adjusting the balance between the generation rate of Cu_2O nanoparticles and the escape rate of solvent [34, 50].

With respect to the micellar systems (e. g. the systems with a Triton X-100 content of 25 and 70 wt%), they are so soft that the generated UO_2 and/or $U(OH)_4$ nanoparticles may not be well adsorbed and aggregated on the surface, and solid nanospheres are synthesized. According to the above discussion, a palisade layer with a suitable strength is helpful to the deposition and aggregation of nanoparticles on its surface. If the palisade layer does not break, nanorod or nanowire will generate.

4 Conclusions

Hollow nanospheres (ϕ: 60–80 nm, wall thickness: 10–20 nm), consisted of UO_2 nanoparticles (ϕ: 3–5 nm), were successfully prepared in a Triton X-100-water (50 : 50, w/w) hexagonal LLC by γ-irradiation, where water soluble AUC was added as precursor. The product was stable at least up to 300 °C. Furthermore, whether the nanospheres were hollow or not, and the wall thickness of the hollow nanospheres could be easily controlled *via* adjusting dose

rate, which will be propitious to investigating the effect of wall thickness on the catalytic activity of hollow uranium oxides nano/microspheres in the future. In the formation course of hollow UO_2 nanospheres, there were three processes (i. e. adsorption, aggregation and fracturing). Meanwhile, the deposition and uneven aggregation of the generated nanoparticles on the surface of the palisade layers of the hexagonal LLC played a key role. While in the Triton X-100 based micellar systems, only solid nanospheres were obtained.

To the best of our knowledge, this is the first report about the hollow uranium oxides nano/microspheres, making the morphologies of uranium oxides more abundant, and the hollow UO_2 nanospheres are the first hollow nano/microspheres synthesized in LLC systems. It is believed that the results reported herein will not only favor the exploration in the field of catalysis with uranium oxides as catalyst, but also afford us some new understanding about the template effect of LLCs.

Acknowledgments: This work was supported by National Natural Science Foundation of China (Grant 91226112), and the Specialized Research Fund for the Doctoral Program of Higher Education of China (Grant no. 20110001120121). Sincere thank are due to Mr. Deliang Sun and Mr. Jiuqiang Li for assistance in the γ-irradiation experiments. We also thank Dr. Jinglin Xie for help with the XPS analyses.

References

1. Hutchings, G. J., Heneghan, C. S., Hudson, I. D., Taylor, S. H.: Uranium-oxide-based catalysts for the destruction of volatile chloro-organic compounds. Nature **384**, 341 (1996).
2. Chong, S. V., Griffiths, T. R., Idriss, H.: Ethanol reactions over the UO_2(111) single crystal: effect of the Madelung potential on the reaction selectivity. Surf. Sci. **444**, 187 (2000).
3. Madhavaram, H., Idriss, H.: Evidence of furan formation from acetaldehyde over β-UO_3. Catal. Today **63**, 309 (2000).
4. Zhang, Z. T., Konduru, M., Dai, S., Overbury, S. H.: Uniform formation of uranium oxide nanocrystals inside ordered mesoporous hosts and their potential applications as oxidative catalysts. Chem. Commun. **20**, 2406 (2002).
5. Wang, Q., Li, G. D., Xu, S., Li, J. X., Chen, J. S.: Synthesis of uranium oxide nanoparticles and their catalytic performance for benzyl alcohol conversion to benzaldehyde. J. Mater. Chem. A **18**, 1146 (2008).
6. Pradhan, M., Sarkar, S., Sinha, A. K., Basu, M., Pal, T.: Morphology controlled uranium oxide hydroxide hydrate for catalysis, luminescence and SERS studies. CrystEngComm **13**, 2878 (2011).
7. Wu, H., Yang, Y., Cao, Y. C.: Synthesis of colloidal uranium-dioxide nanocrystals. J. Am. Chem. Soc. **128**, 16522 (2006).
8. Hudry, D., Apostolidis, C., Walter, O., Gouder, T., Courtois, E., Kübel, C., Meyer, D.: Non-aqueous synthesis of isotropic and anisotropic actinide oxide nanocrystals. Chem. Eur. J. **18**, 8283 (2012).
9. Hudry, D., Apostolidis, C., Walter, O., Gouder, T., Courtois, E., Kübel, C., Meyer, D.: Controlled synthesis of thorium and uranium oxide nanocrystals. Chem. Eur. J. **19**, 5297 (2013).
10. Zhao, R., Wang, L., Gu, Z., Yuan, L., Xiao, C., Zhao, Y., Chai, Z., Shi, W.: A facile additive-free method for tunable fabrication of UO_2 and U_3O_8 nanoparticles in aqueous solution. CrystEngComm **16**, 2645 (2014).
11. Wang, L., Zhao, R., Gu, Z., Zhao, Y., Chai, Z., Shi, W.: Growth of uranyl hydroxide nanowires and nanotubes by the electrodeposition method and their transformation to one-dimensional U_3O_8 nanostructures. Eur. J. Inorg. Chem. **7**, 1158 (2014).
12. Wang, L., Zhao, R., Wang, C., Yuan, L., Gu, Z., Xiao, C., Wang, S., Wang, X., Zhao, Y., Chai, Z., Shi, W.: Template-free synthesis and mechanistic study of porous three-dimensional hierarchical uranium-containing and uranium oxide microspheres. Chem. Eur. J. **20**, 12655 (2014).
13. Lou, X. W., Archer, L. A., Yang, Z.: Hollow micro-/nanostructures: synthesis and applications. Adv. Mater. **20**, 3987 (2008).
14. Hu, Y., Jensen, J. O., Zhang, W., Cleemann, L. N., Xing, W., Bjerrum, N. J., Li, Q. F.: Hollow spheres of iron carbide nanoparticles encased in graphitic layers as oxygen reduction catalysts. Angew. Chem.-Int. Edit. **53**, 3675 (2014).
15. Chen, J., Wang, D. W., Qi, J., Li, G. D., Zheng, F. Y., Li, S. X., Zhao, H. J., Tang, Z. Y.: Monodisperse hollow spheres with sandwich heterostructured shells as high-performance catalysts via an extended SiO_2 template method. Small **11**, 420 (2015).
16. Chen, Y., Ma, P., Gui, S.: Cubic and hexagonal liquid crystals as drug delivery systems. Biomed. Res. Int. **2014,** 12 pages (2014), Article ID 815981.
17. Yamauchi, Y., Kuroda, K.: Rational Design of Mesoporous Metals and Related Nanomaterials by a Soft-Template Approach. Chem. -Asian J. **3**, 664 (2008).
18. Wang, C., Chen, D., Jiao, X.: Lyotropic liquid crystal directed synthesis of nanostructured materials. Sci. Technol. Adv. Mater. **10**, 023001 (2009).
19. Makino, S., Yamauchi, Y., Sugimoto, W.: Synthesis of electrodeposited ordered mesoporous RuO_x using lyotropic liquid crystal and application toward micro-supercapacitors. J. Power Sources **227**, 153 (2013).
20. Ghanem, M. A., Al-Mayouf, A. M., Singh, J. P., Abiti, T., Marken, F.: Mesoporous nickel/nickel hydroxide catalyst using liquid crystal template for ethanol oxidation in alkaline solution. J. Electrochem. Soc. **162**, H453 (2015).
21. Zhou, M., Lin, M., Chen, L., Wang, Y., Guo, X., Peng, L., Guo, X., Ding, W.: Thickness-dependent SERS activities of gold nanosheets controllably synthesized via photochemical reduction in lamellar liquid crystals. Chem. Commun. **51**, 5116 (2015).
22. Li, Q. H., Li, P., Zhang, X.: Synthesis of silver nanorods using lamellar liquid crystal of protic ionic liquids. Asian J. Chem. **25**, 10410 (2013).
23. Zhu, Y., Guo, X., Jin, J., Shen, Y., Guo, X., Ding, W.: Controllable synthesis of CuS nanotubes and nanobelts using lyotropic liquid crystal templates. J. Mater. Sci. **42**, 1042 (2007).
24. Zhu, Y., Guo, X., Mo, M., Guo, X., Ding, W., Chen, Y.: In situ synthesis of horizontally aligned metal–boron alloy nanotubes on a silicon substrate with liquid crystal template. Nanotechnol. **19**, 405 (2008).

25. Zhang, J., Han, B., Li, W., Zhao, Y., Hou, M.: Reversible switching of lamellar liquid crystals into micellar solutions using CO_2. Angew. Chem. Int. Ed. **47**, 10119 (2008).
26. Chen, Q. D., Shen, X. H., Gao, H. C.: Radiolytic syntheses of nanoparticles in supramolecular assemblies. Adv. Colloid Interf. Sci. **159**, 32 (2010).
27. Belloni, J.: Nucleation, growth and properties of nanoclusters studied by radiation chemistry - Application to catalysis. Catal. Today **113**, 141 (2006).
28. Jiang, X., Xie, Y., Lu, J., Zhu, L. Y., He, W., Qian, Y. T.: Simultaneous in situ formation of ZnS nanowires in a liquid crystal template by γ-irradiation. Chem. Mater. **13**, 1213 (2001).
29. Nenoff, T. M., Jacobs, B. W., Robinson, D. B., Provencio, P. P., Huang, J., Ferreira, S., Hanson, D. J.: Synthesis and low temperature in situ sintering of uranium oxide nanoparticles. Chem. Mater. **23**, 5185 (2011).
30. Roth, O., Hasselberg, H., Jonsson, M.: Radiation chemical synthesis and characterization of UO_2 nanoparticles. J. Nucl. Mater. **383**, 231 (2009).
31. Rath, M. C., Naik, D. B., Sarkar, S. K.: Reversible growth of UO_2 nanoparticles in aqueous solutions through 7 MeV electron beam irradiation. J. Nucl. Mater. **438**, 26 (2013).
32. Chen, Q. D., Shen, X. H.: Formation of mesoporous $BaSO_4$ microspheres with a larger pore size via ostwald ripening at room temperature. Cryst. Growth Des. **10**, 3838 (2010).
33. He, P., Shen, X. H., Gao, H. C.: Size-controlled preparation of Cu_2O octahedron nanocrystals and studies on their optical absorption. J. Colloid Interf. Sci. **284**, 510 (2005).
34. Chen, Q. D., Shen, X. H., Gao, H. C.: Formation of solid and hollow cuprous oxide nanocubes in water-in-oil microemulsions controlled by the yield of hydrated electrons. J. Colloid Interface Sci. **312**, 272 (2007).
35. Zhou, J., Zhao, H. K., Shi, J. F., Chen, Q. D., Shen, X. H.: Radiolytic synthesis of prismatical $PbSO_4$ microcrystals. Radiat. Phys. Chem. **97**, 366 (2014).
36. Wu, K.: The solubility of ammonium uranyl tricarbonate (AUC). Atomic Energy Sci. Technol. **3**, 148 (1961).
37. Beyer, K.: Phase structures,water binding, and molecular-dynamics in liquid-crystalline and frozen states of the system Triton X-100-D_2O: a deuteron and carbon NMR-study. J. Colloid Interface Sci. **86**, 73 (1982).
38. Jiang, W., Yu, B., Liu, W., Hao, J.: Carbon nanotubes incorporated within lyotropic hexagonal liquid crystal formed in room-temperature ionic liquids. Langmuir **23**, 8549 (2007).
39. Zhang, J., Xie, Z., Hill, A. J., She, F. H., Thornton, A. W., Hoang, M., Kong, L. X.: Structure retention in cross-linked poly(ethylene glycol) diacrylate hydrogel templated from a hexagonal lyotropic liquid crystal by controlling the surface tension. Soft Matter **8**, 2087 (2012).
40. Song, G., Han, J., Bo, J., Guo, R.: Synthesis of polyaniline nanostructures in different lamellar liquid crystals and application to lubrication. J. Mater. Sci. **44**, 715 (2008).
41. Yan, Y., Jia, X., Meng, M., Qu, C.: Foam superstabilization by lamellar liquid crystal gels. Chem. Lett. **40**, 261 (2011).
42. Celik, O., Dag, O.: A new lyotropic liquid crystalline system: Oligo(ethylene oxide) surfactants with $M(H_2O_n)X^{m-}$ transition metal complexes. Angew. Chem.-Int. Edit. **40**, 3800 (2001).
43. Allen, G. C., Holmes, N. R.: Surface characterization of α-UO_3, β-UO_3, γ-UO_3, and δ-UO_3 using X-ray photoelectron-spectroscopy. J. Chem. Soc. Dalton **12**, 3009 (1987).
44. Idriss, H.: Surface reactions of uranium oxide powder, thin films and single crystals. Surf. Sci. Rep. **65**, 67 (2010).
45. Guilbert, S., Guittet, M. J., Barre, N., Gautier-Soyer, M., Trocellier, P., Gosset, D., Andriambololona, Z.: Dissolution of UO_2 in boom clay water in oxidizing conditions: an XPS study. J. Nucl. Mater. **282**, 75 (2000).
46. Wei, W., Wang, Z., Liu, Z., Liu, Y., He, L., Chen, D., Umar, A., Guo, L., Li, J.: Metal oxide hollow nanostructures: Fabrication and Li storage performance. J. Power Sources **238**, 376 (2013).
47. Sasidharan, M., Nakashima, K.: Core–shell–corona polymeric micelles as a versatile template for synthesis of inorganic hollow nanospheres. Accounts Chem. Res. **47**, 157 (2014).
48. Dong, Y., Qing, Y., Qing, Huang, Y.: Textures and disclinations in the cholesteric liquid-crystalline phase of a cyanoethyl chitosan solution. J. Polym. Sci. Polym. Phys. **38**, 980 (2000).
49. Buxton, G. V., Greenstock, C. L., Helman, W. P., Ross, A. B.: Critical-review of rate constants for Rraction of hydrated electrons, hydrogen-atoms and hydroxyl radicals(.OH/.O-) in aqueous-solution. J. Phys. Chem. Ref. Data **17**, 513 (1988).
50. Luo, F., Wu, D., Gao, L., Lian, S. Y., Wang, E. B., Kang, Z. H., Lan, Y., Xu, L.: Shape-controlled synthesis of Cu_2O nanocrystals assisted by triton X-100. J. Cryst. Growth **285**, 534 (2005).

Supplemental Material: The online version of this article (DOI: 10.1515/ract-2016-2626) offers supplementary material, available to authorized users.